# Similarity evaluation of 3D topological measurement results using statistical methods (Rising Researcher)

Suresh, Vignesh, Zheng, Yi, Zhang, Xiao, Wang, Shaodong, Qin, Hantang, et al.

Vignesh Suresh, Yi Zheng, Xiao Zhang, Shaodong Wang, Hantang Qin, Qing Li, Beiwen Li, "Similarity evaluation of 3D topological measurement results using statistical methods (Rising Researcher)," Proc. SPIE 11397, Dimensional Optical Metrology and Inspection for Practical Applications IX, 113970A (21 April 2020); doi: 10.1117/12.2557627

SPIE.

Event: SPIE Defense + Commercial Sensing, 2020, Online Only

# Similarity evaluation of 3D topological measurement results using statistical methods

Vignesh Suresh[1] , Yi Zheng[1] , Xiao Zhang[2] , Shaodong Wang[2] , Hantang Qin[2] , Qing Li[2] and Beiwen Li[1,*]

[1]Department of Mechanical Engineering, Iowa State University.
[2]Department of Industrial and Manufacturing Systems Engineering, Iowa State University.

## ABSTRACT

Three dimensional (3D) topology data obtained from different optical metrology techniques tend to produce local disagreements which may yield incorrect judgement from inspectors especially under scenarios of precision metrology. This research explores statistical methods to provide a functional scoring for similarities. The investigation is conducted using two statistical methods (Pearsons correlation coefficient and image distance), two optical techniques (structured light and focus variation microscopy) and two application scenarios (metal additive printing and ballistic forensic examination). Experimental results show the promise of using statistical tools to assist binary decisions for matching/non-matching even if 3D topology data are obtained from different optical techniques.

## 1. INTRODUCTION

3D imaging techniques have been widely used in many fields such as automobile, manufacturing, and entertainment industries. These methods are mainly used for quality inspection. One of the recent advancements in the manufacturing industry is Additive Manufacturing (AM)[1] technique. In this method, the part is manufactured by printing layer by layer. In order to avoid defects between the layers, quality inspection needs to be done. This requires an inspection system which can obtain the 3D topography of the sample surface without causing any damage to it. Therefore, non-contact 3D imaging techniques can be used for performing quality inspection of AM parts.

Non-contact optical 3D shape measurement methods such as laser triangulation,[2] stereo vision,[3] and structured light system (SLS)[4] have been successful in obtaining the 3D topographical information of the object. However, there is a local disagreement among the different scanning systems mainly because of their working principle, which results in different topographical data of the sample when scanned using different optical systems. This might create a problem between the upstream and downstream manufacturers in a cyber-manufacturing system. If the upstream and downstream manufacturer uses different optical systems for inspecting the shape of the part, they might have different topographical information once they share the results in the cyber-space. This will lead to disagreement in the quality of the parts. Another application scenario will be in the case of ballistic forensic examinations. Each bullet will have a unique signature (a permanent change in the surface topography) when it is fired from the gun .[5,6] This can be very useful in a crime scene to identify whether two bullets were fired from the same gun. So the ballistic experts need to check for the similarity between the bullet's topography scanned by different systems. Therefore, there needs to be a method to check the similarity of the parts scanned using different optical systems.

Researchers have proposed some methods in the past for estimating the similarity between different optical systems. Surface roughness obtained from different optical systems was used as a metric to evaluate similarity among the different scanning systems.[7,8] However, surface roughness depends on one cross-section line, and it does not represent the entire data set. Launhardt et al.[9] proposed to use the arithmetic mean height of the samples for comparison. Though the method makes use of all the data points, it might neglect the geometrical distribution of the data points. Therefore, there needs to be a method to evaluate the similarity of the surfaces using the geometrical distribution of the data.

In this research, we propose to make use of the topography data obtained from different optical scanning systems for evaluating the similarity between them. We have used two statistical methods for comparing the 3D point-cloud data sets from different systems - Pearson's correlation coefficient (PCC) [10] and image distance method.[11] The optical systems that we have used in this research are focus variation microscopy (FVM) and structured light system (SLS). We have evaluated

* beiwen@iastate.edu; https://www.me.iastate.edu/faculty/?user_page=beiwen.

Dimensional Optical Metrology and Inspection for Practical Applications IX, edited by Kevin G. Harding, Song Zhang, Proc. of SPIE Vol. 11397, 113970A · © 2020 SPIE · CCC
code: 0277-786X/20/$21 · doi: 10.1117/12.2557627

the similarity between three AM samples and between two bullet samples. The method involves scanning the sample using the two optical systems and registering the two 3D data sets using Iterative Closest Point (ICP) [12,13] and k-nearest regression .[14] The topographical map is obtained from the registered 3D data sets and is evaluated for similarity using PCC and image distance method. The proposed method has the advantage of evaluating the similarity using the entire three-dimensional data set and is also flexible in comparing systems with different resolutions. The paper is organized as follows: Section 2 introduces the principle of the two optical systems, data registration, and the two statistical point-cloud data comparison methods. Section 3 describes the experiments that we conducted using the proposed method. Section 4 summarizes the paper.

## 2. PRINCIPLES

In this section, the fundamental principles of SLS and FVM will be introduced. Then, the 3D data alignment process will be introduced. Finally, the proposed 3D point cloud data similarity evaluation method will be discussed.

### 2.1 Principle of optical methods

#### 2.1.1 Structured light system

The Structured light system is a non-contact 3D measurement method. Figure 1 represents the principle of the structured light system. Here A represents a projector pixel, D represents a camera pixel, and the B is the point on the object being scanned. The projector projects preloaded codified fringe patterns on the object. These patterns get distorted based on the topography of the object. These distorted fringe patterns are captured by a camera. The camera images are then used to reconstruct the 3D image (of the objects topography) by using the correspondence established between the projector and camera. The main advantage of SLS is that unlike other methods (such as stereo vision), there is no problem of establishing correspondence pairs. The codifications in the fringe patterns help to establish a better correspondence between the projector and camera. In this research, we have attached a telecentric lens to the camera to achieve a high accuracy 3D shape measurement.

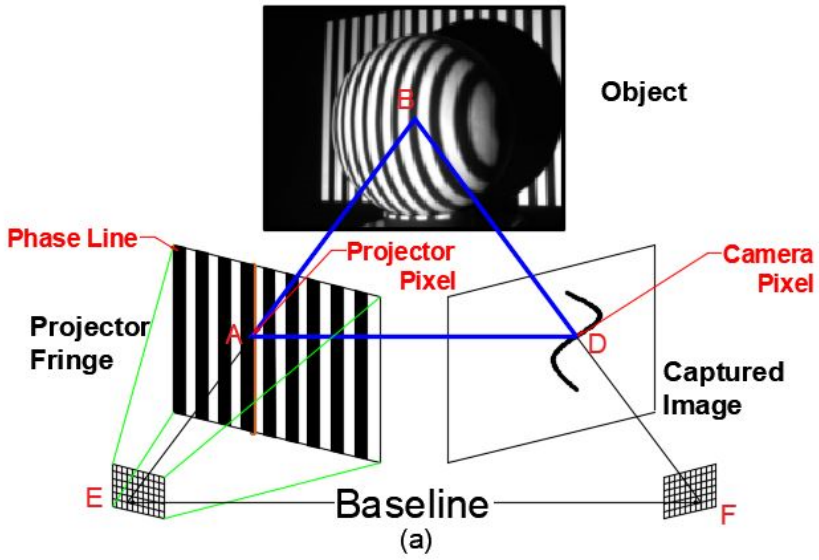


Figure 1: A schematic diagram of structured light system

#### 2.1.2 Focus variation microscopy

Focus variation microscopy is another non-contact 3D measurement method that obtains the surface topography of the sample by varying the focus levels.[15] The principle of the FVM is illustrated in Fig. 2. The light from the light source is transmitted through the beam splitter and then to the sample surface through the objective lens. Based on the sample's

topography, the light will get reflected in different directions. Some parts of the reflected light will be collected by the objective lens and then passed on to the camera sensor. In order to obtain the best focusing location of the optical element pointing to the specimen, a driving unit is used. This process is used to generate a depth map of the sample for different lateral locations.

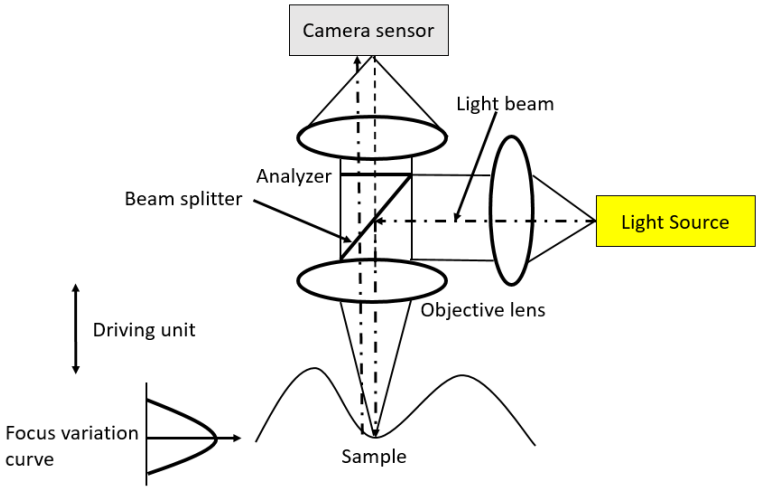


Figure 2: A schematic diagram of focus variation microscopy

### 2.1.3 Data processing

The 3D geometrical information of the sample scanned using the two optical systems will be in the form of 3D point-cloud data set. This point-cloud data set cannot be directly used for evaluating the similarity as the field-of-view, and the data formatting of the two data sets are different. Therefore, the two data sets need to be processed. The data processing mainly involves data registration and data resampling. The schematic of our proposed framework is illustrated in Fig. 3

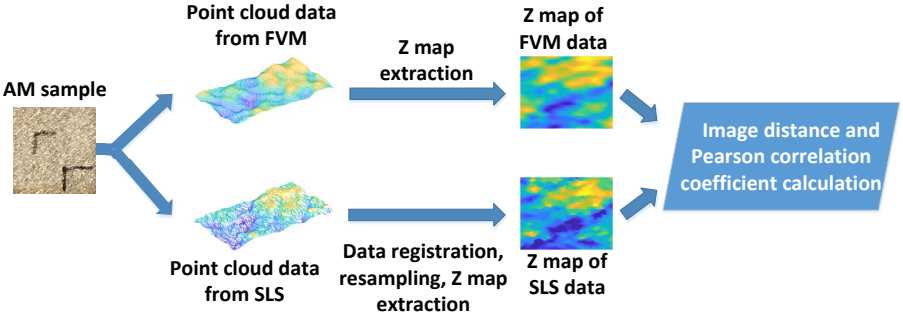


Figure 3: A schematic diagram of proposed 3D point-cloud data comparison method

First, the 3D data sets are aligned by the Iterative Closest Point (ICP) algorithm.[15,16] The reference point-cloud data is denoted as $P$, and the point-cloud that needs to be transformed and aligned with $P$ is $Q$, the ICP algorithm first finds all correspondence point pairs and stores them in a set $\kappa = \{(p,q)|p \in P, q \in Q\}$. Then, an objective function $E(T)$ will be minimized by updating the corresponding point pairs $\kappa$, rotation matrix $R$ and translation vector $t$ iteratively. This objective function is defined as the sum of the squared Euclidean distances after transformation:

$$E(T) = \sum_{(p,q)\in\kappa} ||p - (R \cdot q + t)||^2 \tag{1}$$

The refined rotation matrix $R$ and translation vector $t$ will be obtained after the iterations. Then, this transformation matrix can be used to closely align the two point-cloud data sets.

Second, the 3D data points should be in the same format to avoid confusion while evaluating the similarity. In the case of FVM, the 3D data, is obtained by direct depth retrieval via focus analysis, where the lateral data positions (X and Y) are well-formatted in a raster order of camera pixels. The pixels will be equally spaced in the X-Y plane like that of an evenly spaced mesh grid shown in Fig. 4. Each corner point (highlighted in green color) in the grid represents a point on the 3D point-cloud data set. But in case of SLS, the points will not be evenly spaced as it uses triangulation to obtain the 3D coordinates (X, Y, and Z) of the sample being scanned. Therefore, the lateral data positions (X and Y) are not formatted in a raster order, similar to a mesh grid. To address this challenge, we propose to transform all 3D point-cloud data sets into

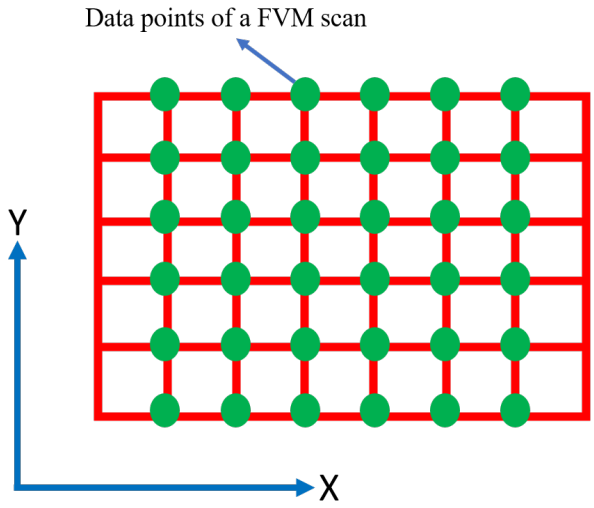


Figure 4: A schematic representation of the raster format of the data points in FVM

an image space, where the locations of all data points are aligned as mesh grid with the index of the image pixels as labels. This transformation process is only for the 3D data set obtained from SLS data. The transformation process is similar to data-resampling, where the query points lie on a given mesh grid defined by the region of interest, and the point-clouds coordinates are the sample values. The heights of the query points can be retrieved by interpolation. At a query point $P_q(X_q, Y_q, Z_q)$, $X_q$ and $Y_q$ are the horizontal coordinates given by the mesh grid, $Z_q$ can be interpolated by a weighted mean of $k$ nearest points to $(X_q, Y_q)$. These points are denoted as $\rho = \{P_i(X_i, Y_i, Z_i)\}$. The weights are assigned as:

$$\omega_i = \frac{1}{\sigma\sqrt{2\pi}} \exp\left(-\frac{d_i^2}{2\sigma^2}\right) \tag{2}$$

Where $d_i$ is the Euclidean distance between $(X_q, Y_q)$ and $(X_i, Y_i)$. Finally, $Z_q$ can be interpolated by

$$Z_q = \frac{1}{k} \sum_{P_i \in \rho} \omega_i \cdot Z_i \tag{3}$$

The point-cloud is denser than the mesh grid so there is no need of any interpolation. With this transformation the SLS 3D point-cloud data set will be transformed into the same depth-coded image space with well-aligned mesh grid.

### 2.1.4 Statistical methods for comparing point-cloud data sets

In this section, we will describe the two statistical methods used for evaluating the similarity between the two 3D data sets.
*Pearson's correlation coefficient*
Let $M$ by $N$ denote the dimensions of the two depth-coded images. This matrix can be transformed into two $M \times N$ vectors

($I_1$ and $I_2$) by connecting each row. The similarity of the two vectors can be estimated by computing the PCC of the two vectors. The PCC parameter can be mathematically defined as:

$$r = \frac{\sum_{i=1}^{M\times N}(I_1^i - \overline{I_1})(I_2^i - \overline{I_2})}{\sqrt{\sum_{i=1}^{M\times N}(I_1^i - \overline{I_1})^2}\sqrt{\sum_{i=1}^{M\times N}(I_2^i - \overline{I_2})^2}} \tag{4}$$

Where $I_1^i$, $I_2^i$ are the values of $i$ th dimension of the vectors $I_1$ and $I_2$; $\overline{I_1} = \frac{1}{M\times N}\sum_{i=1}^{M\times N} I_1^i$(the mean). The result $r$ will range from -1 to 1. If two images are very similar, then the value of $r$ will be close to 1. If the images are different, the value will be close to $-1$.

### 2.1.5 Image distance

Image distance is another method to evaluate the similarity of two images.[11] If the images are similar, then the output will be equal to 0. The method involves converting the two images ($M$ by $N$ pixels) into two $M \times N$ vectors ($I_1$ and $I_2$). The image distance between the two vectors can be defined as:

$$d(I_1, I_2) = [(I_1 - I_2)^T G(I_1 - I_2)]^{\frac{1}{2}} \tag{5}$$

where $G$ is a $M \times N$ by $M \times N$ matrix,

$$G = (g_{ij})_{M\times N * M\times N} \tag{6}$$

and the elements in $G$ are:

$$g_{ij} = f(|P_i - P_j|), i, j = 1, 2...M \times N$$

where $|P_i - P_j|$ is the distance between $i^{th}$ pixel and $j^{th}$ pixel in the image. The function $f$ is defined as:

$$f(|P_i - P_j|) = \frac{1}{\sqrt{2\pi\sigma}} \exp(-\frac{|P_i - P_j|^2}{\sigma^2}) \tag{7}$$

where $\sigma$ is a hyperparameter and can be set to any positive number. If two pixels $P_i$ and $P_j$, are spaced apart then the distance between them will be a large value resulting in smaller values of $g_{ij}$. It will contribute significantly to the total image distance. Therefore, the algorithm is robust to small deformations.

## 3. EXPERIMENT

To evaluate the accuracy of our proposed similarity evaluation method, we used two optical systems, a FVM and a SLS system for 3D topographical scanning. The FVM system uses a microscopic camera to capture images of the samples. The resolution of the camera is set to 1920 $\times$ 1200. The depth resolution of the FVM is 1.1 $\mu$. The SLS system consists of a DLP development kit (model: DLP Lightcrafter 4500, native resolution 910 $\times$ 1140 pixels) and a CMOS camera. The resolution of the camera is set to 1280 $\times$ 960. A telecentric lens with a magnification of 0.486 is attached to the camera. The depth resolution of the SLS is 10 $\mu$. The system is calibrated based on the method described by Li and Zhang.[17] We tested the algorithm with two different samples - AM parts (as shown in Fig. 5(a)-5(c)) and bullets (as shown in Fig. 6(a)). Both the samples were scanned using the two optical systems, and their corresponding 3D point-cloud data sets were evaluated for similarity. The 3D point-cloud data of the AM and bullet samples from the two optical systems is shown in Fig. 5 and Fig. 6, respectively.

First, the similarity/difference between the two 3D point-cloud data sets was estimated using the PCC criteria for all the samples. We used three AM samples and two bullets for the experiment. The process basically involves scanning of the three AM samples using the two optical systems and labeling the 3D data sets of the same sample from the different system as similar using the two statistical methods. The same goes for the bullet samples. The similarity evaluation results of the AM samples and bullets are illustrated in Fig. 7 and Fig. 8, respectively. From Fig. 7 (a) and Fig. 8 (a), since the PCC values on the main diagonal are computed using the exact same point-cloud data (self-comparison), the values will be one. The values around the main diagonal line are the PCC values calculated for the measured data of the same sample using different optical systems (highlighted with blue color). We can observe that these values are significantly larger than the rest (non-highlighted ones), which indicates the similarities of different samples. For better visualization, we have plotted

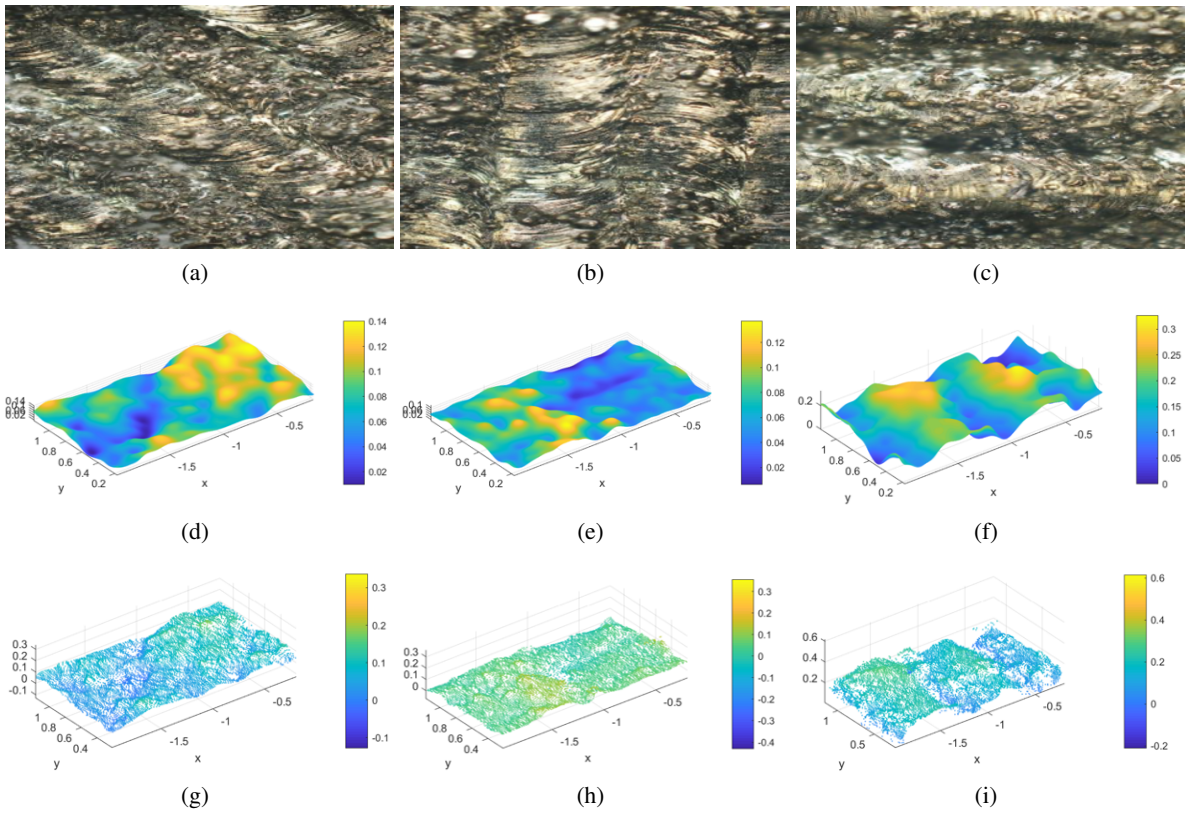

(a) (b) (c)

(d) (e) (f)

(g) (h) (i)

Figure 5: (a) - (c) Snapshot of additive manufactured sample surface; (d) - (f) 3D point cloud data obtained from FVM and (g) - (i) 3D point cloud data obtained from SLS.

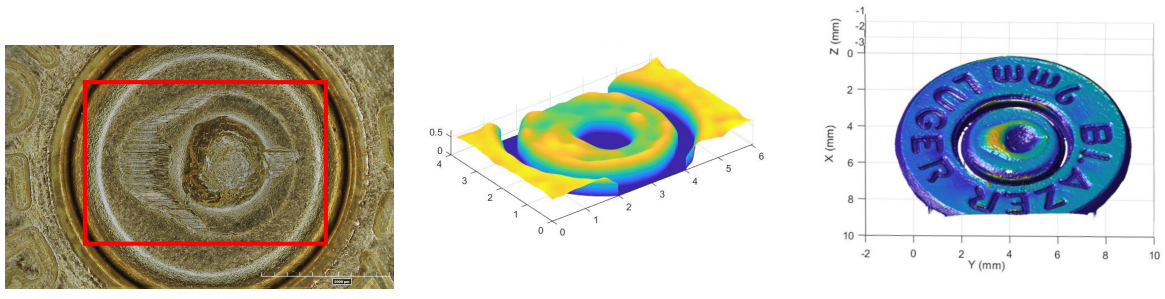


(a) (b) (c)

Figure 6: (a) Snapshot of bullet sample surface; (b) 3D point cloud data obtained from FVM and (c) 3D point cloud data obtained from SLS.

a histogram for all values in this matrix. We can observe that there is a clear gap between the two groups of computed PCC values. The group of small values is the data pairs that come from different samples, and the group of large values is the data pairs from the same samples. The results demonstrate that PCC is very useful in identifying whether two 3D point-cloud data sets correspond to the same sample surface, though they may be scanned using different optical systems.

| | SLS sample 1 | FVM sample 1 | SLS sample 2 | FVM sample 2 | SLS sample 3 | FVM sample 3 |
|---|---|---|---|---|---|---|
| SLS sample 1 | 1 | 0.7947 | -0.3949 | -0.2849 | -0.1502 | -0.0608 |
| FVM sample 1 | 0.7947 | 1 | -0.4017 | -0.3317 | -0.1359 | -0.0630 |
| SLS sample 2 | -0.3949 | -0.4017 | 1 | 0.6029 | 0.2664 | 0.1945 |
| FVM sample 2 | -0.2849 | -0.3317 | 0.6029 | 1 | 0.0019 | 0.1287 |
| SLS sample 3 | -0.1502 | -0.1359 | 0.2664 | 0.0019 | 1 | 0.6635 |
| FVM sample 3 | -0.0608 | -0.0630 | 0.1945 | 0.1287 | 0.6635 | 1 |

(a)

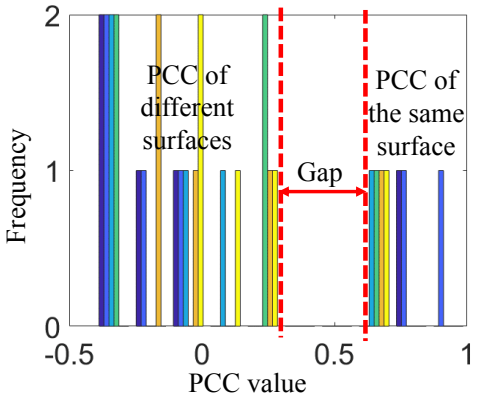


(b)

Figure 7: (a) Confusion matrix of PCC values for 3D point-clouds from Samples 1 - 3 measured by FVM and SLS; (b) Corresponding histogram for PCC values in (a).

| | Gun 1 bullet 1 | Gun 1 bullet 2 | Gun 2 bullet 1 | Gun 3 bullet 1 |
|---|---|---|---|---|
| Gun 1 bullet 1 | 1 | 0.9204 | 0.3432 | 0.2583 |
| Gun 1 bullet 2 | 0.9204 | 1 | 0.3094 | 0.167 |
| Gun 2 bullet 1 | 0.3432 | 0.3094 | 1 | 0.3161 |
| Gun 3 bullet 1 | 0.2583 | 0.167 | 0.3161 | 1 |

(a)

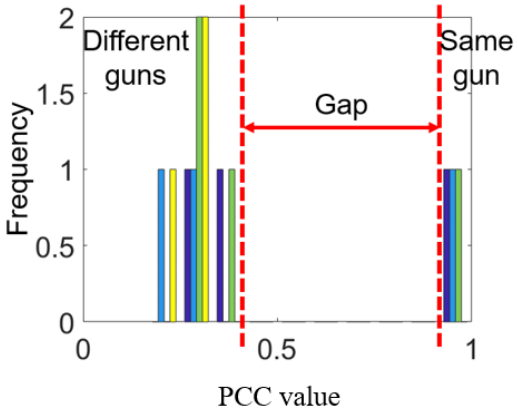


(b)

Figure 8: (a) Confusion matrix of PCC values for 3D point-clouds of two bullet samples measured by FVM and SLS; (b) Corresponding histogram for PCC values in (a).

Second, we computed the image distance values between different 3D point-cloud data sets and arranged them in the matrix, as shown in Fig. 9 and Fig. 10 (a). All the values along the main diagonal are zero as the comparison is within the same data. In the case of data sets obtained from the same sample using different optical systems, the values are significantly smaller than the rest (that are calculated from different surfaces), indicating that these data sets have a smaller image distance between them. In order to have a better visualization, we plotted a histogram (as shown in Fig. 9(b) and Fig. 10(b)), for all the values in the matrix and we can see a clear gap between the two groups of values. Unlike PCC, smaller image distance values indicate that the 3D point-cloud data sets are measured from the same sample, while the group of larger values indicates that the pairs are measured from different samples. The results show that image distance is also useful in identifying whether the measured data are from the same sample even though they are scanned using different optical systems.

| | SLS sample 1 | FVM sample 1 | SLS sample 2 | FVM sample 2 | SLS sample 3 | FVM sample 3 |
|---|---|---|---|---|---|---|
| SLS sample 1 | 0 | 134.562 | 356.088 | 336.272 | 319.358 | 310.287 |
| FVM sample 1 | 134.562 | 0 | 356.489 | 341.961 | 317.104 | 310.216 |
| SLS sample 2 | 356.088 | 356.489 | 0 | 179.401 | 252.992 | 269.965 |
| FVM sample 2 | 336.272 | 341.961 | 179.401 | 0 | 290.522 | 274.520 |
| SLS sample 3 | 319.358 | 317.104 | 252.992 | 290.522 | 0 | 167.139 |
| FVM sample 3 | 310.287 | 310.216 | 269.965 | 274.520 | 167.139 | 0 |

(a)

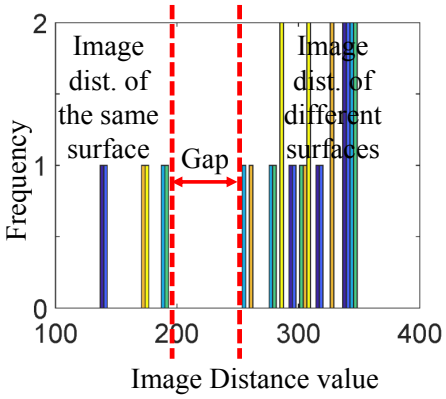


(b)

Figure 9: (a) Confusion matrix of image distance values for 3D point-clouds of Samples 1 - 3 measured by FVM and SLS; (b) Corresponding histogram for image distance values in (a).

| | Gun 1 bullet 1 | Gun 1 bullet 2 | Gun 2 bullet 1 | Gun 3 bullet 1 |
|---|---|---|---|---|
| Gun 1 bullet 1 | 0 | 4.231 | 13.55 | 10.66 |
| Gun 1 bullet 2 | 4.231 | 0 | 13.82 | 10.03 |
| Gun 2 bullet 1 | 13.55 | 13.82 | 0 | 13.69 |
| Gun 3 bullet 1 | 10.66 | 10.03 | 13.69 | 0 |

(a)

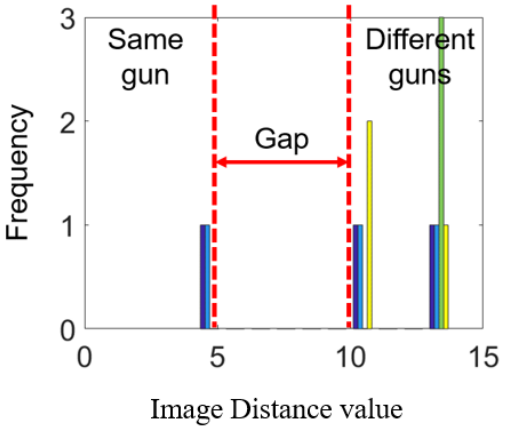


(b)

Figure 10: (a) Confusion matrix of image distance values for 3D point-clouds of two bullet samples measured by FVM and SLS; (b) Corresponding histogram for image distance values in (a).

## 4. CONCLUSION

This research proposes a method to evaluate similarities between two 3D point-cloud data sets of the same sample obtained from different optical metrology systems. After scanning the samples using the two optical systems, the two point-cloud data sets are registered using ICP and then transformed into one unified image space. We have used two statistical methods (PCC and image distance) to evaluate the similarity of the 3D data sets. From the experimental results, we can observe that our proposed method can well distinguish if a pair of 3D point-cloud data sets are measured from the same sample, even though they were obtained from two optical systems with different spatial resolutions or fields-of-view.


## Acknowledgments

The authors would like to thank the support from Research Experience of Undergraduates (REU): Lara Chunko, Kelsey Benjamin and Jennifer Patterson. This work is supported by the U.S. Department of Energys Office of Energy Efficiency and Renewable Energy (EERE) under the Advanced Manufacturing Office Award Number DE-EE0007897, and National Science Foundation (# 1757900).

## REFERENCES


[1] Senin, N., Thompson, A., and Leach, R. K., "Characterisation of the topography of metal additive surface features with different measurement technologies," *Measurement Science and Technology* **28**(9), 095003 (2017).

[2] Tay, C. J., Wang, S. H., Quan, C., and Shang, H. M., "In situ surface roughness measurement using a laser scattering method," *Optics Communications* **218**, 1–10 (2003).

[3] Zhongxiang, H., Lei, Z., Jiaxu, T., Xuehong, M., and Xiaojun, S., "Evaluation of three-dimensional surface roughness parameters based on digital image processing," *International Journal of Advanced Manufacturing Technology* **40**, 342–348 (2009).

[4] Li, B. and Zhang, S., "Flexible calibration method for microscopic structured light system using telecentric lens," *Optics Express* **23**, 25795 (2015).

[5] Song, J., "Proposed nist ballistics identification system (nbis) based on 3d topography measurements on correlation cells," *AFTE Journal* **45**(2), 184–194 (2013).

[6] Vorburger, T. V., Yen, J. H., Bachrach, B., Renegar, T. B., Ma, L., Rhee, H.-G., Zheng, X. A., Song, J.-F., and Foreman, C. D., "Surface topography analysis for a feasibility assessment of a national ballistics imaging database," tech. rep. (2007).

[7] Poon, C. Y. and Bhushan, B., "Comparison of surface roughness measurements by stylus profiler, afm and non-contact optical profiler," *Wear* **190**, 76–88 (1995).

[8] Zhang, X., Zheng, Y., Suresh, V., Wang, S., Li, Q., Li, B., and Qin, H., "Correlation approach for quality assurance of additive manufactured parts based on optical metrology," *Journal of Manufacturing Processes* **53**, 310–317 (2020).

[9] Launhardt, M., Wrz, A., Loderer, A., Laumer, T., Drummer, D., Hausotte, T., and Schmidt, M., "Detecting surface roughness on sls parts with various measuring techniques," *Polymer Testing* **53**, 217–226 (2016).

[10] Pearson, K., "Liii. on lines and planes of closest fit to systems of points in space," *The London, Edinburgh, and Dublin Philosophical Magazine and Journal of Science* **2**(11), 559–572 (1901).

[11] Wang, L., Zhang, Y., and Feng, J., "On the euclidean distance of images," *IEEE transactions on pattern analysis and machine intelligence* **27**(8), 1334–1339 (2005).

[12] Chen, Y. and Medioni, G., "Object modelling by registration of multiple range images," *Image and vision computing* **10**(3), 145–155 (1992).

[13] Besl, P. J. and McKay, N. D., "Method for registration of 3-d shapes," in [*Sensor Fusion IV: Control Paradigms and Data Structures*], **1611**, 586–607, International Society for Optics and Photonics.

[14] Altman, N. S., "An introduction to kernel and nearest-neighbor nonparametric regression," *The American Statistician* **46**(3), 175–185 (1992).

[15] Danzl, R., Helmli, F., and Scherer, S., "Focus variation a robust technology for high resolution optical 3d surface metrology," *Strojniki vestnik Journal of Mechanical Engineering* **2011**(03), 245–256 (2011).

[16] Dhond, U. R. and Aggarwal, J. K., "Structure from stereo-a review," *IEEE transactions on systems, man, and cybernetics* **19**(6), 1489–1510 (1989).

[17] Li, B. and Zhang, S., "Flexible calibration method for microscopic structured light system using telecentric lens," *Optics express* **23**(20), 25795–25803 (2015).